Available online at www.sciencedirect.com

SCIENCE DIRECT

Biochimica et Biophysica Acta 1708 (2005) 120–132

BIOCHIMICA ET BIOPHYSICA ACTA BBA

http://www.elsevier.com/locate/bba

Towards a spin coupling model for the Mn_4 cluster in Photosystem II

Marie-France Charlot[a], Alain Boussac[b,1], Geneviève Blondin[a,*]

[a]*Laboratoire de Chimie Inorganique, UMR 8613, LRC-CEA no. 33V, Institut de Chimie Moléculaire et des Matériaux d'Orsay, Université Paris-Sud, 91405 Orsay Cedex, France*

[b]*Service de Bioénergétique, URA CNRS 2096, DBJC, CEA Saclay, 91191 Gif-sur-Yvette, France*

Received 3 November 2004; received in revised form 13 January 2005; accepted 20 January 2005
Available online 2 March 2005

Abstract

The X-band EPR spectra of the IR sensitive untreated PSII and of MeOH- and NH_3-treated PSII from spinach in the S_2-state are simulated with collinear and rhombic *g*- and Mn-hyperfine tensors. The obtained principal values indicate a 1Mn(III)3Mn(IV) composition for the Mn_4 cluster. The four isotropic components of the Mn-hyperfine tensors are found in good agreement with the previously published values determined from EPR and ^{55}Mn-ENDOR data. Assuming intrinsic isotropic components of the Mn-hyperfine interactions identical to those of the Mn-catalase, spin density values are calculated. A Y-shape 4*J*-coupling scheme is explored to reproduce the spin densities for the untreated PSII. All the required criteria such as a S=1/2 ground state with a low lying excited spin state (30 cm^{-1}) and an easy conversion to a S=5/2 system responsible for the g=4.1 EPR signal are shown to be satisfied with four antiferromagnetic interactions lying between −290 and −130 cm^{-1}.

Keywords: Photosystem II; Manganese; EPR spectroscopy; Hyperfine interaction; Spin coupling

1. Introduction

The evolution of oxygen as a result of the light-driven water oxidation is catalysed by Photosystem II (PSII) in which a cluster of four manganese ions acts both as an oxidizing accumulating device and as the active site [1,2]. During the enzyme cycle, the oxidizing side of PSII goes through five different redox states that are denoted S_n, n varying from 0 to 4. Oxygen is released during the S_3 to S_0 transition in which S_4 is a transient state. The structure of the Mn_4 cluster and the mechanism by which water is oxidized are still subject to intense discussions. The resolution of the X-ray structures is improving together with the *R*-factor [3–5] but the chemical nature of the manganese core is not yet definitely established [6,7]. Therefore, investigations based on extended X-ray absorption and electron paramagnetic resonance can still help in the elaboration of the Mn_4 structure and of a water-oxidation mechanism.

The first signal detected from the S_2-state was a multiline signal near g=2 [8]. This signal is spread over roughly 1800 G and is made up of at least 18 lines, each separated by approximately 80 G, and arises from a magnetic tetramer [9–13]. The S_2-state can be quantitatively formed either by flash illumination in non-frozen samples [8] or by continuous illumination at 200 K. Similar S_2-multiline signals have been detected in PSII isolated from plants [8,14–20], from the cyanobacteria, *Thermosynechococcus elongatus* [21–23] and *Synechocystis* PCC 6803 [24–26] and from the green alga, *Scenedesmus obliquus* [27,28].

Under some experimental conditions (in the presence of sucrose in the buffer) the S_2-state gives rise to a g=4.1 signal that is stable at temperatures above 200 K, rather than a multiline signal [29,30]. For this g=4.1, the fraction of centres giving rise to this signal is dependent on the pre-treatment of the enzyme, being markedly increased by, (i) having sucrose present in the medium [30,31], (ii) certain

* Corresponding author. Tel.: +33 1 69 15 47 55; fax: +33 1 69 15 47 54.
E-mail addresses: alain.boussac@cea.fr (A. Boussac), gblondin@icmo.u-psud.fr (G. Blondin).
[1] Tel.: +33 1 69 08 72 06; fax: +33 1 69 08 87 17.

0005-2728/$ - see front matter © 2005 Elsevier B.V. All rights reserved.
doi:10.1016/j.bbabio.2005.01.006

treatments which remove chloride from the medium [32,33] or its replacement by F^- [29,34], I^-, [34, 35] amines [36] or NO_3^-, [34], (iii) replacing Ca^{2+} with Sr^{2+} [37]. This g=4.1 signal is suppressed by the presence of alcohols [30].

The g=4.1 state can also be formed preferentially by illumination below 200 K if the light used is not free of infrared radiation [38]. The absorption of radiation at ≈820 nm by the Mn_4-cluster induces a transition between a S=1/2 state into a $S \geq 5/2$ state irrespective, at least below 200 K, of the temperature at which the sample is illuminated [38–41]. At temperatures equal to or lower than 77 K, a state responsible for EPR signals with g-values higher than 5 is trapped. Between 77 and 150 K, an activation barrier can be overcome and the next stable state becomes that responsible for the g=4.1 signal [40]. At temperatures higher than 150 K, the stable state is that responsible for the S_2-multiline signal [40].

In untreated PSII from plants, two populations of PSII reaction centres have been defined based on the behaviour of the S_2-state versus IR illumination: those centres in which the spin state is changed by IR light and those centres which are insensitive to IR light [42]. The total S_2-multiline signal results from the superposition of the two types of multiline signals that originate from these two PSII populations. The S_2-population that is insensitive to IR light gives rise to a "narrow" multiline signal characterized by stronger central lines and weaker outer lines. The IR sensitive S_2-population gives rise to a "broad" multiline signal in which the intensity of the outer lines, at low and high fields, is larger relative to those in the narrow multiline signal. Methanol addition to plant PSII results in a significantly different S_2-multiline signal [21,43]. The spectral properties of the methanol S_2-multiline signal were found to correspond to PSII centres which are insensitive to IR light and indeed, the yield of the IR-induced spin conversion in the S_2-state in the presence of methanol was close to zero [21]. In the presence of methanol the Mn_4-structure in PSII from plants appears therefore to be more homogenous as measured by its sensitivity to IR light.

The hyperfine structure of the S_2-state EPR signal is a fingerprint of the electronic structure of the tetranuclear manganese cluster. Consequently, simulations of the multiline spectrum have been performed to determine how the electronic density is spread on the four metallic sites [10,11,44–47].

In this work, we will present simulations of three X-band EPR spectra of the S_2-state. The first one is associated with the IR-sensitive population of PSII from spinach. The second and third spectra are produced after MeOH or NH_3 treatments of the enzyme, respectively. As detailed below, no hypothesis concerning neither the oxidation states of the manganese ions nor a magnetic coupling scheme is formulated. The sole assumption is the S=1/2 spin value associated with the investigated signals. Collinear and rhombic g- and Mn-hyperfine tensors are deduced and further analysed. In the case of the IR-susceptible population of untreated PSII samples, a 1Mn(III)3Mn(IV) composition for the Mn_4 cluster is found. To reproduce the *isotropic* components of the hyperfine tensors, a 4J-magnetic coupling scheme is explored to concommitantly locate the Mn(III) ion and evaluate the $\{J_{ij}\}$-set. Results are discussed in comparison with previously published works.

2. Experimental section

2.1. PSII preparations

PSII preparations and the generation of the S_2-state multiline spectra were done as previously described [37,38,42,48].

2.2. EPR spectroscopy

All spectra were recorded at 9 K on a Bruker ESR300 X-band spectrometer equipped with an Oxford ESR 900 helium cryostat, a Hewlett-Packard 5350B frequency counter, and a Bruker 035M NMR gaussmeter.

2.3. EPR simulation techniques

Simulations of the EPR spectra were performed using a FORTRAN program which calculates the powder spectra of systems with S=1/2 ground state taking into account the hyperfine interactions of the manganese nuclei with nuclear spin I=5/2 [49]. For each transition, the resonant field is calculated by using perturbation theory up to the second order for the hyperfine interactions. The resulting stick spectrum is then convoluted with Gaussian functions of fixed width (half-width at half-height) δB. This simulation program is coupled to a minimisation program in order to find the set of parameters giving the lowest possible value of the agreement R-factor defined from experimental and calculated intensities according to Eq. (1).

$$R = \frac{\sum_i \left(I_i^{\exp} - I_i^{\mathrm{calc}}\right)^2}{\sum_i \left(I_i^{\exp}\right)^2} \tag{1}$$

We consider as adjustable parameters the three principal values of the g-tensor and the three principal values of each effective hyperfine tensor that is assumed to be collinear with the g-tensor. This corresponds to a 15-parameter fit.

3. Methods for simulating EPR spectra

The spin-Hamiltonian for a system of n coupled paramagnetic ions is [50]:

$$\boldsymbol{H}_{\mathrm{spin}} = \sum_{i=1}^{n} \{\mu_B \boldsymbol{B}[\boldsymbol{g}_i]\boldsymbol{S}_i + \boldsymbol{I}_i[\boldsymbol{a}_i]\boldsymbol{S}_i + \boldsymbol{S}_i[\boldsymbol{D}_i]\boldsymbol{S}_i\} - \sum_{\substack{i,j=1 \\ i<j}}^{n} J_{ij}\boldsymbol{S}_i \cdot \boldsymbol{S}_j \tag{2}$$

The sum runs over all paramagnetic ions; in the case of PSII it is at most four and we will retain n=4 throughout this paper. In brackets, the three terms are, starting from the left: the electronic Zeeman term, the electron-nuclear hyperfine interaction and the zero-field splitting term of each metallic site. The last term in Eq. (2) represents the isotropic magnetic exchange interaction between the four paramagnetic Mn ions. In this equation, $\boldsymbol{B}$ is the external magnetic field, μ_B the Bohr magneton, $[\boldsymbol{g_i}]$ the g-tensor of ion i, $\boldsymbol{S_i}$ the electronic spin operator of ion i, $\boldsymbol{I_i}$ the nuclear spin operator of ion i, $[\boldsymbol{a_i}]$ the local hyperfine tensor for the interaction of $\boldsymbol{S_i}$ and $\boldsymbol{I_i}$ on the same centre, $[\boldsymbol{D_i}]$ the zero-field splitting tensor of ion i. We will further neglect the nuclear Zeeman and the quadrupolar terms, as usual in all works not dealing with ^{55}Mn-ENDOR, except in the simulations performed by Åhrling and Pace [51].

The hyperfine term is meaningful in the interpretation of the EPR spectra. Generally speaking, it reflects the interaction that exists on one atom between the nuclear and the electronic magnetic moments. The former is directly proportional to the nuclear spin of the element (I=5/2 for Mn ions). The latter is governed by the distribution of the unpaired electrons of the manganese ions over all individual atomic sites. This means that the electronic spin density is spread over the metallic sites only (the small delocalisation onto the ligands is neglected) and depends on the nature and the strength of the exchange interactions between the paramagnetic centres.

If one assumes that among the four terms written in Eq. (2), the exchange interaction between the metallic sites is the preponderant effect, one can deduce an energetic scheme in which (i) the levels are labelled by the total spin angular momentum S and (ii) the separation between levels is governed by the coupling constants J_{ij}. Each state is completely described by the individual electronic spins S_i, the total spin S and the relative values of the J_{ij} interactions [50].

The low-temperature observed EPR spectra involve the lowest of these states which is in the present study a S=1/2 state [52,53]. For this state we can write the following effective spin Hamiltonian [50]:

$$\boldsymbol{H}_{\text{eff}} = \mu_B \boldsymbol{B}[\boldsymbol{g}]\boldsymbol{S} + \sum_{i=1}^{4} \boldsymbol{I}_i[\boldsymbol{A}_i]\boldsymbol{S} \tag{3}$$

In this expression, $[\boldsymbol{g}]$ and $[\boldsymbol{A_i}]$ are the effective tensors related to the S=1/2 total spin state. Each of them can be expressed in terms of the real uncoupled corresponding ones written in Eq. (2). For instance, when local zero-field splitting effects are neglected, the effective hyperfine tensor $[\boldsymbol{A_i}]$ of ion i is related to the intrinsic hyperfine tensor $[\boldsymbol{a_i}]$ by the relationship:

$$[\boldsymbol{A_i}] = \rho_i[\boldsymbol{a_i}] \tag{4}$$

ρ_i is the spin density on site i which describes the ground state studied; it is a scalar quantity that depends on the total spin quantum number S, the four individual S_j-spins ($1 \leq j \leq 4$), that is the oxidation state of all the ions constituting the magnetic cluster, and the J_{ij}/J_{kl}-ratios. J_{kl} designates one specific non-zero exchange interaction among the $\{J_{ij}\}$-set. Eq. (4) shows that the effective and the local hyperfine tensors have the same principal axes. The same relation holds between the x, y or z components of each tensor as well as between their isotropic parts, $A_{i,\text{iso}}=(A_{i,x}+A_{i,y}+A_{i,z})/3$ and $a_{i,\text{iso}}=(a_{i,x}+a_{i,y}+a_{i,z})/3$, respectively. The scalar quantities ρ_i are calculated according to the rules stated for the addition of angular momenta in quantum mechanics [54]. At this stage, we recall that it is only for a dinuclear system that the spin densities ρ_i (i=1, 2) do not depend on the coupling constant between the two magnetic ions, provided that it is negative to ensure the S=1/2 spin state to be the ground state. For localized mixed-valence Mn(III)Mn(IV) systems one has $[\boldsymbol{A_{III}}]=2[\boldsymbol{a_{III}}]$ and $[\boldsymbol{A_{IV}}]=-[\boldsymbol{a_{IV}}]$ for the Mn(III) and Mn(IV) sites, respectively.

If in Eq. (2) one (or more) zero-field splitting interaction is no longer negligible but remains small compared to the energy gap between the ground and the first excited states determined according to the exchange Hamiltonian, the ground state is a Kramer's doublet, that is a two-fold degenerated level for which the remaining degeneracy can only be removed under the action of an external magnetic field. This ground Kramer's doublet can be considered as an effective S=1/2 system. The electronic properties can be reproduced by the effective Hamiltonian in Eq. (3) but the relation between the effective and the local hyperfine tensors has to be expressed according to Eq. (5):

$$[\boldsymbol{A_i}] = [\rho_i][\boldsymbol{a_i}] \tag{5}$$

where $[\rho_i]$ is the spin density matrix. For small zero-field splitting interactions, the matrix can be calculated using perturbation theory. In addition to the S- and S_j-spin quantum numbers ($1 \leq j \leq 4$) and the J_{ij}/J_{kl}-ratios, the matrix depends on the zero-field splitting tensors $[\boldsymbol{D_j}]$ [50]. The spin density matrices are thus anisotropic and the effective hyperfine tensor $[\boldsymbol{A_i}]$ would have the same principal directions as the local hyperfine tensor $[\boldsymbol{a_i}]$ only under the assumption that the four zero-field tensors $[\boldsymbol{D_j}]$ ($1 \leq j \leq 4$) are collinear to $[\boldsymbol{a_i}]$. The influence of the Mn(III) zero-field splitting has been exposed by several authors for dinuclear complexes [46,55–59] but only one investigation has been performed for a tetranuclear cluster [46]. In the following, the spin densities will be evaluated from the isotropic part of the hyperfine tensors. This allows to neglect the zero-field splitting effects and to rely on Eq. (4) for the relation between effective and local hyperfine tensors.

Eqs. (3) and (4) represent the starting point for each research which intends to gain information from the EPR spectra. Additional assumptions must be clearly explained.

At first, the nuclearity – strictly speaking, the magnetic nuclearity – of the cluster responsible for the multiline signal must be specified. Although all experimental evidences have shown that a Mn_4 cluster is present in PSII,

Table 1
Effective g- and Mn-hyperfine principal values obtained from the simulation of the S_2-state EPR spectrum of untreated PSII

Model	[g][a]		[A_1] (MHz)	[A_2] (MHz)	[A_3] (MHz)	[A_4] (MHz)	Method
Zheng [45]			III	III	III	IV	B
	⊥	2.01	−277	−277	+226	+250	
	//	1.97	−363	−363	+288	+226	
	iso	*1.997*	*−306*	*−306*	*+247*	*+242*	
	aniso	*0.04*	*86*	*86*	*62*	*24*	
Zheng [45]			IV	III	IV	IV	B
	⊥	2.00	−280	−257	+237	+237	
	//	1.98	−300	−337	+237	+237	
	iso	*1.993*	*−287*	*−284*	*+237*	*+237*	
	aniso	*0.02*	*20*	*80*	*0*	*0*	
Peloquin [64]	⊥	1.99	−285	+255	+255	−195	A
	//	1.95	−310	+205	+205	−180	
	iso	*1.977*	*−293*	*+238*	*+238*	*−190*	
	aniso	*0.04*	*25*	*50*	*50*	*15*	
Hasegawa [44]			IV	III	IV	IV	B
	x	1.993	295	291	248	110	
	y	1.990	304	284	233	106	
	z	1.976	294	194	245	117	
	iso	*1.986*	*298*	*257*	*242*	*111*	
	aniso	*0.017*	*11*	*90*	*15*	*11*	
This work	*x*	1.988	324	240	248	181	A
	y	1.985	351	306	263	184	
	z	1.975	312	225	217	193	
	iso	*1.983*	*329*	*257*	*243*	*186*	
	aniso	*0.013*	*39*	*81*	*46*	*12*	

[a] x, y and z are the principal axes ordered according to the decreasing order of the [g] principal values; *iso* is the isotropic component (see text); *aniso* is the absolute value of the difference between the maximum and the minimum values of the principal components.

Åhrling and Pace [51] have supposed that this spectrum is produced by a dinuclear system with large nuclear quadrupolar interactions and unusual coordination of the manganese ions. We have previously discarded this hypothesis [9] and ^{55}Mn-ENDOR studies have definitely rejected it [46]. We thus no longer retain this possibility. In the following, we will suppose that the four Mn ions are in sufficiently closed magnetic exchange in order to include four hyperfine interactions as suggested by the recently published X-ray structures.

At this stage, two alternate strategies are possible.

(A) In a first approach, effective parameters can be obtained from a fit of the EPR spectrum using Eq. (3). Only absolute values of the hyperfine principal values can be determined. No assumption is made whatever the coupling scheme. The effective hyperfine constants will be reproduced assuming a magnetic topology only in a second independent step. The expression "magnetic topology" means the package of the oxidation states of the manganese sites that is the four S_j-values ($1 \leq j \leq 4$), together with the number and strength of the magnetic interactions that is the $\{J_{ij}\}$-set.

(B) Another approach consists in using some previous information on the local hyperfine tensors of the Mn(III) and Mn(IV) ions, as deduced for instance from the study of dinuclear systems, and to calculate the effective hyperfine tensors according to Eq. (4). This means that a magnetic coupling scheme is elaborated with local spin values and a given set of J_{ij}-coupling constants. The experimental spectrum is then simulated by means of Eq. (3) and an adjustment of the g-tensor. *It is worth noticing that any assumption made in the coupling scheme will inevitably be underlying in the calculated effective hyperfine tensors*.

In both approaches, the symmetries of the g- and Mn-hyperfine tensors have to be specified. Isotropic tensors that were assumed in the first studies [9,60,61] are unrealistic and have no longer been used in the recent works. When assuming axial or rhombic symmetries, all tensors are supposed to have the same principal directions (collinear tensors), except in the study of Hasegawa et al. [44]. This hypothesis seems reasonable if there is only one Mn(III) ion and if the Mn(IV) coordination spheres are not too distorted. When non-collinear tensors are assumed, Euler angles smaller than 6° are obtained for PSII [44] while 8° is the upper value determined for dinuclear Mn(III)Mn(IV) complexes [57]. Such small quantities do not justify the further introduction of Euler angles in the simulation of X-band EPR powder spectra.

The principal difference between approaches A and B lies in the step where the magnetic topology of the Mn_4 cluster is introduced. As far as the exchange interactions are preponderant, the effective hyperfine tensors determined according to approach A are indicative of the oxidation degree of the manganese ions. The oxidation state of the cluster which is thus a conclusion of the EPR simulation in

Table 2
Effective g- and Mn-hyperfine principal values obtained from the simulation of the S_2-state EPR spectrum of MeOH-treated PSII

Model	[g][a]		[A_1] (MHz)	[A_2] (MHz)	[A_3] (MHz)	[A_4] (MHz)	Method
Peloquin [46]	⊥	1.97	−311	−232	+200	+180	A
	//	1.99	−270	−270	+250	+240	
	iso	*1.977*	*−297*	*−245*	*+217*	*+200*	
	aniso	*0.02*	*41*	*42*	*50*	*60*	
This work	*x*	1.989	329	287	243	218	A
	y	1.987	305	254	258	188	
	z	1.977	339	224	213	167	
	iso	*1.985*	*324*	*255*	*238*	*191*	
	aniso	*0.012*	*34*	*63*	*45*	*39*	

[a] x, y and z are the principal axes ordered according to the decreasing order of the [g] principal values; *iso* is the isotropic component (see text); *aniso* is the absolute value of the difference between the maximum and the minimum values of the principal components.

Table 3
Effective g- and Mn-hyperfine principal values obtained from the simulation of the S_2-state EPR spectrum of NH_3-treated PSII

Model	$[g]$[a]		$[A_1]$ (MHz)	$[A_2]$ (MHz)	$[A_3]$ (MHz)	$[A_4]$ (MHz)	Method
Zheng [45]			III	IV	III	III	B
	⊥	1.97	−295	−322	+173	+173	
	//	2.01	−385	−294	+227	+227	
	iso	*1.983*	*−325*	*−313*	*+191*	*+191*	
	aniso	*0.04*	*90*	*28*	*54*	*54*	
Peloquin [46]	*x*	1.99	−295	+222	+208	−150	A
	y	1.99	−315	+222	+208	−150	
	z	1.96	−390	+172	+158	−112	
	iso	*1.98*	*−333*	*+205*	*+191*	*−137*	
	aniso	*0.03*	*95*	*50*	*50*	*38*	
This work	*x*	1.989	360	242	211	159	A
	y	1.987	290	210	194	140	
	z	1.958	368	164	168	112	
	iso	*1.978*	*339*	*206*	*191*	*137*	
	aniso	*0.031*	*78*	*78*	*43*	*47*	

[a] x, y and z are the principal axes ordered according to the decreasing order of the $[g]$ principal values; *iso* is the isotropic component (see text); *aniso* is the absolute value of the difference between the maximum and the minimum values of the principal components.

approach A is an assumption in approach B. Furthermore, the magnetic topology assumed in approach B is often chosen in such a way that, in addition to the total spin S, one of the S_{mn}-spin pair is a good quantum number, that is to say some of the exchange J_{ij}-constants are equal [45,47]. The symmetry introduced in the coupling scheme reflects upon the spin densities ρ_i and consequently on the effective hyperfine tensors.

Approach A is the framework of the results reported here. The starting point of the analysis is the simulation of the EPR signal of the S_2-state according to Eq. (3) within rhombic symmetry. The obtained effective g- and Mn-hyperfine tensors are summarised in Tables 1–3 for the untreated and MeOH- and NH_3-treated PSII, respectively, along with those previously reported in the literature with some information concerning the methods used. Results of earlier isotropic simulations have been excluded as well as those of Lakshmi et al. where three out of four metallic sites are considered equivalent. The framework we use here doesn't allow us to specify the signs of the hyperfine constants or the oxidation states of the manganese ions. However, this information is given by some authors and is reported here as published.

4. Analysis of hyperfine parameters deduced from EPR simulations

Before commenting on the values reported in Tables 1–3, we briefly expose here the strategy adopted to analyse the effective hyperfine parameters deduced from the EPR simulations (second step of approach A). We have previously used a similar method in the study of a synthetic tetranuclear model of the Oxygen Evolving Complex [49]. It consists in calculating the spin densities according to a spin-coupling model and in finding values as close as possible to the ones deduced from the isotropic components of the effective hyperfine tensors according to Eq. (4).

4.1. From the effective hyperfine couplings to the experimental spin projections

The first step is the estimation of the spin projections on the manganese ions starting from the isotropic component of the effective hyperfine tensors. By definition, the spin density ρ_i is the ratio between the value of the spin operator $\boldsymbol{S}_{i,z}$ of site i averaged on the ground state function (designated as the spin projection) and the value of the spin operator $\boldsymbol{S}_z$ of the whole cluster averaged on the same function:

$$\rho_i = \frac{\langle \boldsymbol{S}_{i,z} \rangle_{\mathrm{GS}}}{\langle \boldsymbol{S}_z \rangle_{\mathrm{GS}}} \tag{6}$$

If one is interested in the ground state function characterized by S=1/2 and M_S=+1/2, the average value of $\boldsymbol{S}_z$ that corresponds to the spin projection M_S thus gives +1/2. Together with Eq. (4), one gets:

$$A_{i,\mathrm{iso}} = 2a_{i,\mathrm{iso}} \langle \boldsymbol{S}_{i,z} \rangle_{\mathrm{GS}} \tag{7}$$

From the isotropic component $A_{i,\mathrm{iso}}$ of each effective hyperfine tensor it is thus possible to determine the spin projection on each manganese site if we know the isotropic component $a_{i,\mathrm{iso}}$ of the local hyperfine tensor. Our choice focuses on a metalloprotein system rather than on synthetic complexes and catalase was hence selected. In addition, it ensures a more oxygenated surrounding of the manganese ions. We use the intrinsic hyperfine values obtained by Zheng and Dismukes in a simulation of the EPR spectrum of the Mn(III)Mn(IV) form of the catalase from *Thermus thermophilus* [56]. The isotropic values are −192 MHz for Mn(III) and −237 MHz for Mn(IV). Similar values have been determined by Haddy et al. [62] and recently confirmed by the collection and the simulation of the high-field and high-frequency EPR spectrum [63]. Based on the oxidation states of the manganese ions deduced from the effective hyperfine tensors (see later), Eq. (7) then gives the absolute value of the four spin projections, because the signs of the effective hyperfine interactions are not determined from the EPR simulation. Since we are interested in the total spin projection M_S=+1/2, the sum of all the individual spin projections has to give back this value. This allows the attribution of the sign to each experimental spin projection $\langle \boldsymbol{S}_{i,z} \rangle_{\mathrm{GS}}$. The correct distribution, if any, is the one that leads to a sum value close to +1/2.

Taking into account the uncertainties in the simulations and in the values of the intrinsic hyperfine coupling

constants, we add a margin of ±5% on each spin projection. This gives us a set of four spin projection ranges $\langle \boldsymbol{S}_{i,z} \rangle_{GS}$ deduced from the experimental spectrum. Here the subscript i refers to the site labelling which concerns the EPR simulation and runs from 1 to 4.

4.2. From magnetic interactions to calculated spin projections

Starting from a different point of view, we consider now that the OEC cluster is constituted by four manganese ions that interact magnetically according to the exchange Hamiltonian:

$$\boldsymbol{H}_{ex} = -\sum_{\substack{\mu,\nu=\alpha \\ \mu<\nu}}^{\delta} J_{\mu\nu} \boldsymbol{S}_{\boldsymbol{m}} \cdot \boldsymbol{S}_{\boldsymbol{n}} \tag{8}$$

This approach is totally independent of the previous one. So we now designate the magnetic sites with symbol subscripts μ and ν (instead of the i and j subscripts) that may take the values α to δ (instead of 1 to 4). The most general interaction scheme between four paramagnetic sites needs six $J_{\mu\nu}$-coupling constants but this number may be reduced using some knowledge of the system or some hypothesis on the relative values of these couplings. For each magnetic topology corresponding to one given set of $J_{\mu\nu}$-constants, we diagonalise the exchange Hamiltonian of Eq. (8) in the space associated with each total spin S-value. We test if the ground state of the system is a spin doublet and, if true, we calculate the spin projections $\langle \boldsymbol{S}_{\mu,z} \rangle_{GS}$ on each site $\mu(\alpha \leq \mu \leq \delta)$ for which the oxidation degree is known from the magnetic topology being explored.

4.3. Connection between EPR fits and magnetic coupling schemes

Following two different approaches, two sets of spin projections, $\{\langle \boldsymbol{S}_{i,z} \rangle_{GS}\}$ $(1 \leq i \leq 4)$ and $\{\langle \boldsymbol{S}_{\mu,z} \rangle_{GS}\}$ $(\alpha \leq \mu \leq \delta)$ corresponding to the same system are obtained. For the two sets, the oxidation states of the metallic sites are known and the one to one correspondence between sites i and sites μ has to be established. The $\langle \boldsymbol{S}_{\mu,z} \rangle_{GS}$ values in ascending order are tested for belonging to the $\langle \boldsymbol{S}_{i,z} \rangle_{GS}$ ranges (also in increasing order) in a one to one connection (see Fig. 1). We then verify that the corresponding manganese sites i and μ have the same oxidation states. Namely, this reduces to the location of the Mn(III) ion since we will be dealing with a 1Mn(III)3Mn(IV) composition (see below). If it is so, the coupling scheme and the $\{J_{\mu\nu}\}$-set of corresponding exchange coupling constants is retained as a possible model responsible for the EPR spectra.

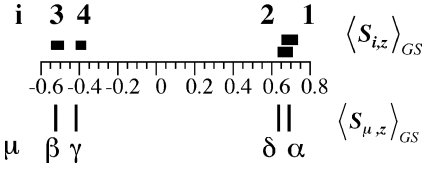

Fig. 1. Connection between experimental spin projection values obtained for untreated PSII within hypothesis 2 with a ±5% margin (see Table 4) and calculated ones with the Mn(III) on site δ and the following $\{J_{\mu\nu}\}$-set (in cm^{-1}): $J_{\alpha\beta}=-225$, $J_{\beta\gamma}=-125$, $J_{\beta\delta}=-170$ and $J_{\gamma\delta}=-130$.

This coupling scheme is not fully determined. We recall here that the spin projections depend on the relative values of the exchange interactions, that is to say on the $J_{\mu\nu}/J_{\kappa\lambda}$-ratios where $J_{\kappa\lambda}$ is one specific non-zero coupling constant. This means that the subscript pair (κ,λ) is fixed while the pair (μ,ν) runs over all possible sets in the tetranuclear system. All the $J_{\mu\nu}$-constants may be expressed as being proportional to this peculiar $J_{\kappa\lambda}$-constant. Thus, the energies associated with this magnetic topology depend only on the $J_{\kappa\lambda}$ exchange interaction. Because the ground state function has been tested to present a total spin $S=1/2$, the sign of $J_{\kappa\lambda}$ is known. We insist on the fact that the absolute value of $J_{\kappa\lambda}$ has no meaning. For instance, in a dinuclear Mn(III)Mn(IV) complex, the spin projections of the $S=1/2$ ground state are +1 and −0.5 whatever the negative value of the exchange interaction. At this stage of the process, we know only the signs of all the exchange constants and their relative strengths but not their values in energy unit (wave numbers for example). To specify them, one has to refer to an energy gap. It is known that in the untreated PSII the first excited state lies 30–40 cm^{-1} above the ground state [11]. For a possible $\{J_{\mu\nu}\}$-set, we calculate the energy of the first excited state and set it to 30 cm^{-1}. This allows us to give the magnetic interaction constants in wave numbers.

Finally, we impose to the $J_{\mu\nu}$-constants to present reasonable values. As known for model manganese complexes with oxo, acetato and N-donor ligands, exchange parameters vary in a wide range; we allow them to lie between −350 and +50 cm^{-1} and retain so the final sets of solutions.

5. Results

5.1. EPR simulations results

Experimental and simulated spectra are reported in Fig. 2. All fits well reproduce the line positions in the central parts of the spectra as well as the overall shape; but the low-intensity lines in the wings are somewhat displaced as is also the case in previously published simulations [44–46].

The principal values of the effective g- and Mn-hyperfine tensors obtained are listed in Tables 1–3 as well as the isotropic part $|A_{i,iso}|$ calculated by assuming a unique sign for the three components. The x, y and z labelling refers to the g principal values given in decreasing order. Sites are labelled (subscripts 1 to 4) according to the isotropic

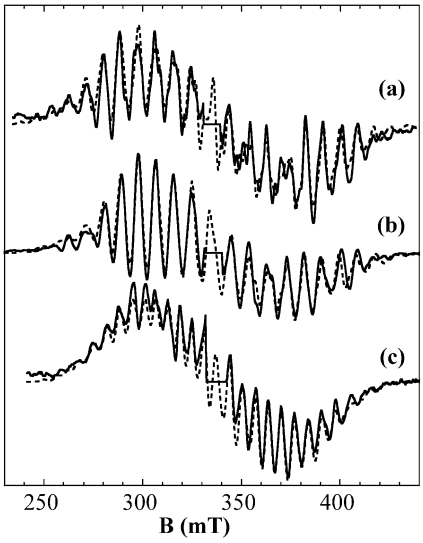

Fig. 2. X-band EPR spectra of PSII (solid lines) and simulated spectra (dashed lines) obtained using a Gaussian line shape with a half-width at half-height δB (agreement factor R calculated according to the text). (a) Untreated PSII: ν=9.421 GHz, T=9 K; Simulation: δB=1.70 mT, R=0.07. (b) MeOH-treated PSII: ν=9.418 GHz, T=9 K. Simulation: δB=1.70 mT, R=0.06. (c) NH_3-treated PSII: ν=9.437 GHz, T=9 K. Simulation: δB=1.75 mT, R=0.03.

components ordered by decreasing absolute values. The positive difference between the utmost components is also reported under the designation *aniso*.

As can be seen from the last line of Table 1, only the hyperfine tensor of site 2 presents a strong anisotropy while the three other centres along with the g-tensor are found almost isotropic. This holds in a lesser extent to the MeOH-treated PSII sample (see Table 2): compared to the untreated PSII sample, sites 2 and 4 are found more rhombic. The presence of a single anisotropic interaction subsequently justifies the collinearity of the g- and Mn-hyperfine tensors. This is clearly not the case for the NH_3-treated PSII particules where an increase in the anisotropy of the g- together with the Mn-hyperfine tensor of site 1 is observed. Consequently, this system will not be further analysed.

Parameters from previously published simulations are also reported in Tables 1–3. The untreated PSII has been the most investigated and an axial symmetry was assumed except by Hasegawa and co-workers. Our results mainly differ from theirs by the stronger components obtained for site 4.

The isotropic part of the Mn-hyperfine tensors of the untreated and the MeOH-treated PSII samples are found very similar. This is in agreement with what was also observed by ^{55}Mn-ENDOR [46,64]. In all samples investigated here, one can see that the isotropic hyperfine values are not far from those of Peloquin et al. in Ref. [46]. This is an important point because their parameters also fit the ^{55}Mn-ENDOR spectra, which is not the case for other works, as they pointed out. Because the following interpretation of the hyperfine interactions resorts on the isotropic part of the tensors, such a similarity in $|A_{i,\mathrm{iso}}|$ ($1 \le i \le 4$) values comforts us in the validity of the parameters obtained here. In the following, we will restrict the analysis to the isotropic hyperfine couplings of the Mn sites of the untreated PSII sample.

As previously mentioned in Section 3, the simulations performed here do not make any assumption on the oxidation state of the manganese ions. Based on X-ray absorption techniques [18,65,66] and on the generation of super-reduced states [67,68], there is a general agreement in the literature on the fact that the S_2-state of the OEC is composed of one Mn(III) and three Mn(IV) ions although this is questioned by some groups [11]. As far as the intrinsic hyperfine interaction is concerned, the Mn(IV) centres are expected to be more or less isotropic while the d^4 configuration of the Mn(III) ion would induce a strong anisotropy. It is noteworthy to see that only one effective hyperfine tensor out of four presents a strong anisotropy for the untreated and the MeOH-treated samples. This is consistent with the 1Mn(III)3Mn(IV) formulation of the Mn_4 cluster of the OEC in the S_2-state and concomitantly strongly suggests that Mn(III) would be located on site 2. Consequently, only the composition 1Mn(III)3Mn(IV) is considered in the following.

5.2. Experimental spin projection values

The spin projection values can be determined according to the procedure described above provided that the Mn(III) ion is located on one of the four sites labelled 1 to 4. Two hypotheses may be formulated. First, the Mn(III) is assumed to be responsible for the strongest effective hyperfine coupling (isotropic component) and is hence located on site 1 (hypothesis 1). Such a situation is observed for the Mn(III) ion in mixed-valence Mn(III)Mn(IV) systems. Second, the Mn(III) is located on site 2 that presents the strongest anisotropic effective hyperfine tensor (hypothesis 2). This is also the case for strongly antiferromagnetically coupled Mn(III)Mn(IV) complexes.

The algebraic values of $\langle \boldsymbol{S}_{i,z} \rangle_{\mathrm{GS}}$ are listed in Table 4. It is astonishing to see that from the absolute values first calculated, a unique combination of signs is possible. Two sites present a positive spin projection, the other two a negative one. Within hypothesis 2, the negative spin projections correspond to sites 3 and 4 that present the smallest spin densities (in absolute value). Note that within this hypothesis, the Mn(III) centre does not present the greatest spin density.

As mentioned previously, the $\pm$5% margin is added to the spin projection values to take into account uncertainties in spin parameters.

5.3. Study of a model magnetic topology

The space of six magnetic exchange coupling constants between the four paramagnetic ions, that is five $J_{\mu\nu}/J_{\kappa\lambda}$-

Table 4
Spin projection values deduced from the EPR simulation of the untreated PSII sample depending on the location of the Mn(III) site (see text)

Site i	1	2	3	4	
$\|A_{i,\mathrm{iso}}\|$ (MHz)	329	257	243	186	
Hypo 1	III	IV	IV	IV	
$\langle \boldsymbol{S}_{i,z}\rangle_{\mathrm{GS}}$	+0.857	+0.542	−0.513	−0.392	+0.494[a]
Hypo 2	IV	III	IV	IV	
$\langle \boldsymbol{S}_{i,z}\rangle_{\mathrm{GS}}$	+0.694	+0.669	−0.513	−0.392	+0.458[a]

[a] The sum of the four spin projections is indicated in the right column.

ratios, is too large to be explored without restrictive starting hypotheses based on a selection of experimental data. Although the resolution of the crystal structures of Photosystem II from either cyanobacterium *T. elongatus* [3] or cyanobacterium *Thermosynechococcus vulcanus* [4] didn't specify the distances in the Mn_4 unit, it shows that the electron density of the manganese cluster is bulged in three directions in the form of a 'Y'. The same motif is also found by Ferreira et al. [5] on the cyanobacterium *T. elongatus*. It has to be noticed that conditions to grow crystals are different from those used to record EPR spectra. The way this influences the structure of the Mn_4 cluster is largely unknown. However, it seemed to us an interesting way to explore a magnetic topology in which the paramagnetic ions are eventually closer together than in the nearly linear magnetic arrangement known as the dimer of dimers of "Klein's model". We propose to study the model including four exchange coupling constants shown in Scheme 1 and we apply it to untreated PSII. Note that Klein's model is included in this 4*J*-coupling scheme if one sets J_{NV} or $J_{NV'}$ to zero.

The experimental spin projections, independent of the coupling scheme, have already been listed in Table 4 and the values including the ±5% margin are reproduced in Fig. 1 for the untreated PSII within hypothesis 2.

In the exchange coupling approach, we firstly locate the Mn(III) ion successively on the three different positions (Extremity, Node or Vertex) of the magnetic structure and then allow each $J_{\mu\nu}$-constant to vary independently in the relative range [−10, +2] in arbitrary unit. We then follow the general method exposed in Section 4.

At the end of the comparison process between experimental and calculated spin densities according to the criteria we have stated, we reach an important conclusion: if we suppose that $|A_{\mathrm{Mn(III),iso}}|$=329 MHz (hypothesis 1), there is no solution (that is to say no $\{J_{\mu\nu}\}$-set) which can reproduce the corresponding $\{\langle \boldsymbol{S}_{i,z}\rangle_{\mathrm{GS}}\}$-set values. On the other hand, we obtain solutions for $|A_{\mathrm{Mn(III),iso}}|$=257 MHz (hypothesis 2) whatever the position (E, N or V) of the Mn(III) ion in the topologic scheme. We shall explore these cases in more details.

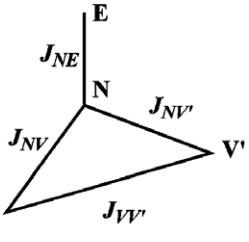

Scheme 1. The investigated Y-shape 4*J*-coupling topology.

First, when the Mn(III) ion is located at the extremity (see Fig. 3), we get solutions with a strong to medium antiferromagnetic coupling J_{NE} in the (III,IV) pair (−350 to −55 cm^{-1}) and a coupling between the two Mn(IV) vertices which is weakly antiferromagnetic (−45 to −15 cm^{-1}). One of the J_{NV} constants must be slightly ferromagnetic (10 to 45 cm^{-1}) and the other J_{NV} constant is medium antiferromagnetic to ferromagnetic (−70 to +20 cm^{-1}). A solution with two simultaneously zero constants is excluded.

When the Mn(III) ion is located at the node of the model (see Fig. 4), the solutions can be divided into two families. The first one appears unrealistic: one of the two (III,IV) pairs connecting the node and a vertex is almost uncoupled (−15 to 0 cm^{-1}) and the other one is ferromagnetically to weakly antiferromagnetically coupled (J_{NV} from −15 to 50

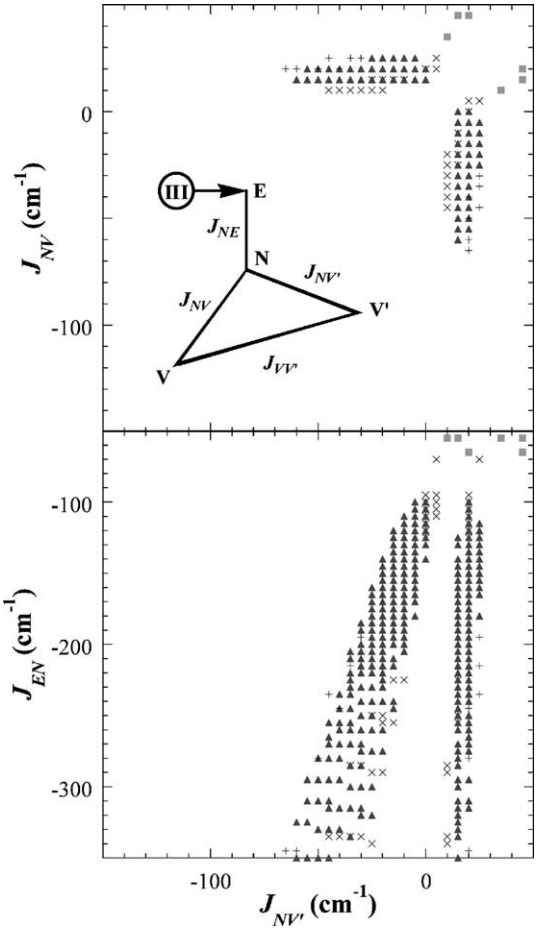

Fig. 3. $\{J_{\mu\nu}\}$-set values solutions of the 4*J*-coupling scheme for the untreated PSII samples with the Mn(III) ion at the extremity. The spin projections are calculated within hypothesis 2. Solutions are plotted as J_{NV} (top) and J_{EN} (bottom) as functions of $J_{NV'}$ with $J_{VV'}$ ranging from −45 to −30 cm^{-1} (■) or equal to −25 (×), −20 (▲) or −15 cm^{-1} (+). All the plotted *J*-constants were approximated to the closest modulus 5 value.

cm^{-1}). In the other family the (IV,IV) pair is strong to medium antiferromagnetic ($J_{VV'}$ from −250 to −50 cm^{-1}), the (III,IV) pair connecting the node to the extremity is weakly antiferromagnetic ($J_{NE} \approx -25$ cm^{-1}) and the other (III,IV) constants connecting the node to the vertices range from −140 to 0 cm^{-1}. However we notice that in such solutions small changes in the J value result in the S=1/2 state to be no longer the ground state.

Finally, when the Mn(III) ion is at a vertex (see Fig. 5), we obtain solutions with all $J_{\mu\nu}$-constants antiferromagnetic and of the same order of magnitude (four strongly antiferromagnetic constants or four intermediate antiferromagnetic ones). Such a magnetic topology with spin frustration on the triangular core allows to spray out the total spin density on the four ions. It also avoids having a high-lying first excited state in spite of the great coupling constants. Furthermore it is likely in a structure with several oxo and carboxylato bridges.

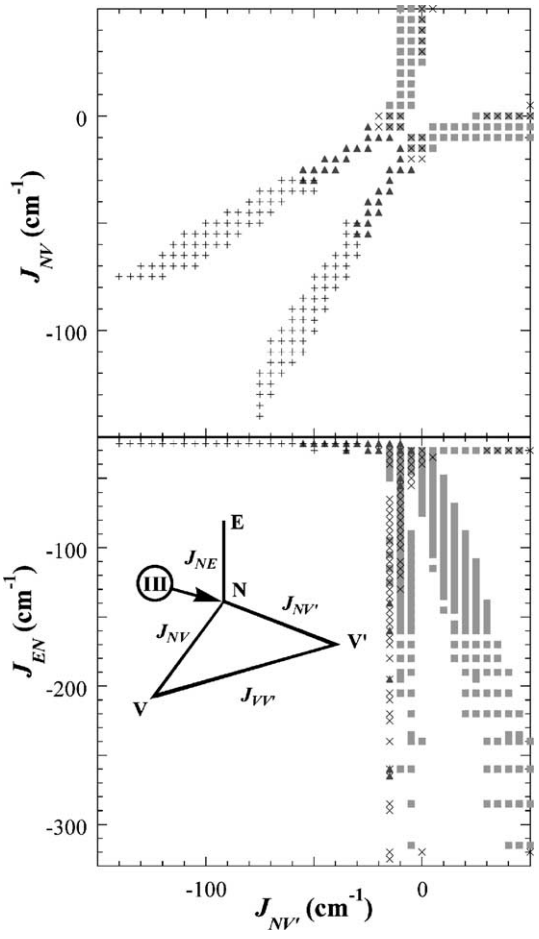

Fig. 4. $\{J_{\mu\nu}\}$-set values solutions of the 4J-coupling scheme for the untreated PSII samples with the Mn(III) ion at the node. The spin projections are calculated within hypothesis 2. Solutions are plotted as J_{NV} (top) and J_{EN} (bottom) as functions of $J_{NV'}$ with $J_{VV'}$ ranging from −25 to −20 cm^{-1} (■), from −35 to −30 cm^{-1} (×), from −100 to −40 cm^{-1} (▲) or from −240 to −105 cm^{-1} (+). All the plotted J-constants were approximated to the closest modulus 5 value.

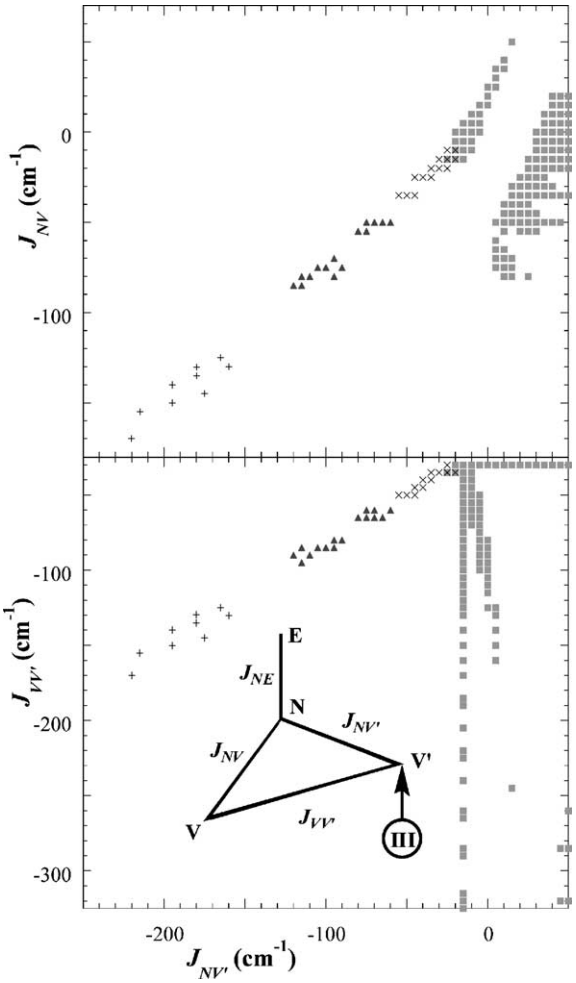

Fig. 5. $\{J_{\mu\nu}\}$-set values solutions of the 4J-coupling scheme for the untreated PSII samples with the Mn(III) ion at the vertex V'. The spin projections are calculated within hypothesis 2. Solutions are plotted as J_{NV} (top) and J_{EN} (bottom) as functions of $J_{NV'}$ with $J_{VV'}$ ranging from −290 to −250 cm^{-1} (■), from −155 to −95 cm^{-1} (×), from −80 to −35 cm^{-1} (▲) or from −30 to −20 cm^{-1} (+). All the plotted J-constants were approximated to the closest modulus 5 value.

We remark that, whatever the location of the Mn(III) ion, the interactions between the extremity and the node and between the two vertices are strictly antiferromagnetic; so a ferromagnetic connection may not be a terminal one in untreated PSII.

6. Discussion

Collinear and rhombic g- and Mn-hyperfine tensors of a S=1/2 system interacting with four I_{Mn}=5/2 nuclear spins were successfully used to simulate S_2-state X-band EPR spectra from untreated and MeOH- and NH_3-treated PSII samples. With the exception of the ammonia treatment, a single tensor is found anisotropic. This is an important result since it subsequently validates the presupposed collinearity of the tensors.

It is worth noticing that most of the previously published simulations assumed axial symmetry with the four Mn-hyperfine tensors sharing the same distortion direction (all the z-axes are parallel). Our choice is less restrictive. For instance, if we take the values reported in Table 1, the four Mn-hyperfine tensors are found close to axial symmetry, with the principal distortion axis aligned along the y-axis for sites 1 and 2 and along the z-axis for sites 3 and 4. Compared to the previous works, we here allow the principal distortion axes of the Mn sites to be perpendicular one to the other.

The elaboration of a magnetic coupling scheme lies on the isotropic parts of the Mn-hyperfine tensors. It has been previously shown for the Mn-catalase that the improvement in the determination of the g-anisotropy using high-field and high-frequency EPR experiments leads to a deviation lower than 3% for the isotropic component of the Mn-hyperfine tensors [63]. In the investigated untreated PSII system, we obtained a g-anisotropy comparable with the ones determined for dinuclear Mn systems from high-field and high-frequency EPR data. The possible deviations on $|A_{i,\mathrm{iso}}|$ originating from the g-anisotropy are in fact considered when including the $\pm 5\%$ margin for the spin densities.

Our approach requires the choice of intrinsic Mn(III) and Mn(IV) hyperfine coupling constant-values. We favour an enzymatic system compared to synthetic models and parameters from the Mn(III)Mn(IV) form of the catalase were thus chosen. From a comparison with synthetic models, the 192 MHz $|a_{\mathrm{Mn(III),iso}}|$-value is smaller than the ones usually found for di-μ-oxo systems with Mn(III) ion in a N_4O_2 environment (205–230 MHz) [57,63,69,70] but is closer to what is found for di-μ-oxo-μ-acetato (195–205 MHz) [57,63] or mono-μ-oxo ($\approx$185–190 MHz) [71,72] compounds. On the reverse, the 237 MHz $|a_{\mathrm{Mn(IV),iso}}|$-value is larger than the reported values for di-μ-oxo (215–225 MHz), di-μ-oxo-μ-acetato (205–215 MHz) and mono-μ-oxo ($\approx$185 MHz) species. These differences may originate from the chemical ligation of the Mn ions. The X-ray structure recently published by Ferreira et al. [5] identified six direct protein ligands for the four manganese ions with five oxygen and one nitrogen coordinating atoms. The remaining coordinations sites are filled by either water, hydroxyls or bicarbonate. The Mn ligands are thus mainly oxygenated.

Several attempts were performed to test the compatibility of possible magnetic topologies with hyperfine couplings, but restrictive hypotheses were always formulated. As previously mentioned, the composition 3Mn(III)1Mn(IV) can be discarded. For the 1Mn(III)3Mn(IV) composition, a linear 3J-coupling model has been explored but deduced from a structural proposal with two di-μ-oxo and one mono-μ-oxo bridges. Therefore, the whole space of J-values is far from being totally investigated [46]. The other tested magnetic topologies included four or more J-constants but assumes the presence of one strongly antiferromagnetically coupled Mn(III)Mn(IV) subunit at least [12,13]. Based on the first published X-ray structures [3,4], we deliberately restrict the magnetic topology to a Y-shape 4J-coupling scheme that includes the "dimer of dimers" model from Klein's group. Within this framework, 4J-sets are indeed obtained that reproduce the calculated spin densities and lead to a S=1/2 ground state with a 30 cm^{-1} first excited spin state. No model accounting for a linear topology with one zero-constant and three strong antiferromagnetic exchange interactions was found suggesting that the so-called "dimer of dimers" model is not appropriate for the S_2-state. In addition, no restriction resorting on the presence of one strongly antiferromagnetically coupled Mn(III)Mn(IV) unit was stated for the J-values. Consequently, some of the solutions plotted here could not be obtained by Hasegawa and coworkers [12,13] despite their impressive work.

Among the proposed magnetic coupling models, a selection can be further performed based on the explanation of the other EPR signatures of the Mn_4-cluster. For instance, the conversion of the multiline spectrum to the g=4.1 signal is a crucial point, as previously mentioned [10–12]. However, it has to be specified that one must refer to the coupling constants expressed in wave numbers rather than in arbitrary units. Starting from the plotted J-values in Figs. 3–5 and assuming the same location for the manganese valences, it was impossible to obtain a S>3/2 ground spin state when allowing the J-constants to vary by $\pm 30\%$. However, a S=5/2 ground spin state can be reached if the Mn(III) ion is located on a neighbouring site. A variation of at most 10% was assigned for the Mn pairs remaining at the IV–IV level, if any, upon the new location of the Mn(III) ion. On the reverse, no restriction was specified for the Mn pairs that change in oxidation state. An example is given in Fig. 6.

Only the isotropic components of the Mn-hyperfine tensors were analysed. Anisotropies were only used to

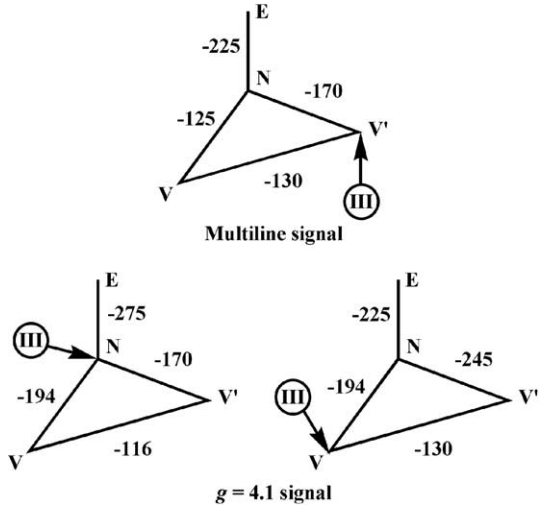

Fig. 6. A pecular $\{J_{\mu\nu}\}$-set (in cm^{-1}) which can produce the multiline signal (top) and two $\{J_{\mu\nu}\}$-sets (in cm^{-1}) with an S=5/2 ground spin-state (bottom). The later are generated by the hop of the Mn(III) site from V' to N or V.

corroborate the 1Mn(III)3Mn(IV) composition. The hyperfine anisotropy of site *i* originates from both the intrinsic hyperfine anisotropy of the Mn ion and the zero-field splitting effects. Using either high-field and high-frequency EPR or parallel detection mode at X-band, a great variety of zero-field splittings were determined for mononuclear Mn(III)-based systems either biological or synthetic, a majority of the axial parameter D being negative [73–82]. Weaker effects are usually found in Mn(IV) systems. As clearly demonstrated for dinuclear systems, the zero-field splitting effect on the Mn(III) centre can be transferred to the adjacent Mn site [46,56,57]. The transfer increases with increasing local $D_{\mathrm{Mn(III)}}$-value and/or decreasing energy gaps between the S=1/2 ground state and the excited spin states. Consequently, the presence of only one strongly anisotropic hyperfine tensor for the untreated PSII sample that presents a low-lying excited spin state (30–40 cm^{-1}) suggests that the zero-field splitting effect on the Mn(III) ion is small. Indeed, when assuming an axial zero-field splitting effect on the Mn(III) ion characterized by a $|D|$-value smaller than 2 cm^{-1}, an exact calculation of the spin density matrices $[\rho_i]$ and consequently of the intrinsic Mn-hyperfine tensor from the effective $[\boldsymbol{A}_i]$-tensor ($1 \le i \le 4$) according to Eq. (5) demonstrates that the local isotropic component $a_{i,\mathrm{iso}}$-values depart from those of the catalase by less than the allowed $\pm 5\%$. On the other hand, two hyperfine tensors for the NH_3-treated sample present similar but high anisotropy. This may indicate a stronger zero-field splitting effect on the Mn(III) site consequently to the ammonia treatment, the separation in energy with the first excited spin state being comparable in both the untreated and NH_3-treated samples (≈ 30 cm^{-1}).

7. Conclusion

S_2-state X-band EPR spectra recorded on untreated and MeOH- and NH_3-treated PSII samples from spinach were successfully simulated. Only the untreated system was further considered. The resulting Mn-hyperfine tensors are indicative of a 1Mn(III)3Mn(IV) composition. Assuming a Y-shape 4J-coupling scheme, the spin densities of the Mn ions determined from the isotropic part of the hyperfine interactions can be reproduced with four intermediate to strong antiferromagnetic exchange couplings (J ranging from -290 to -130 cm^{-1}), as usually determined for Mn-oxo complexes. Among these solutions, we favoured location of the Mn(III) on one vertex.

The X-ray structure recently published by Ferreira et al. is very stimulating. Indeed, the four manganese ions seem to be in an even closer magnetic interaction than the Y-shape 4J-coupling scheme model investigated in this work and a fifth exchange interaction may be present, between sites V and E for instance (see Scheme 1). An analysis of the S=1/2 EPR signature of a new synthetic tetranuclear Mn(III/IV)-based system would be of great help in this respect. The X-ray structure also suggests rich oxygen coordination for the Mn ions. To investigate their hyperfine and zero-field splitting characteristics, the synthesis of polynuclear manganese complexes with N_2O_4, NO_5 or even O_6 surroundings for the metallic ions is a challenge for the inorganic chemists.

Acknowledgements

We are grateful to Dr. Pierre Dorlet, Pr. Jean-Jacques Girerd and Pr. Patrick Bertrand for stimulating discussions. The COST D21 European action and the LRC-CEA project are acknowledged for their financial support.

References

[1] Special issue devoted to Photosystem II, Biochim. Biophys. Acta 1503 (2001).
[2] J. Barber, J.M. Anderson, Philosophical Transactions Issue on Photosystem II: Molecular Structure and Function, The Royal Society, London, 2002.
[3] A. Zouni, H.-T. Witt, J. Kern, P. Fromme, N. Krauß, W. Saenger, P. Orth, Crystal structure of Photosystem II from *Synechococcus elongatus* at 3.8 Å resolution, Nature 409 (2001) 739–743.
[4] N. Kamiya, J.-R. Shen, Crystal structure of oxygen-evolving Photosystem II from *Thermosynechoccus vulcanus* at 3.7 Å resolution, Proc. Natl. Acad. Sci. U. S. A. 100 (2002) 98–103.
[5] K.N. Ferreira, T.M. Iverson, K. Maghlaoui, J. Barber, S. Iwata, Architecture of the photosynthetic oxygen-evolving center, Science 303 (2004) 1831–1838.
[6] A.W. Rutherford, P. Faller, The heart of photosynthesis in glorius 3D, Trends Biochem. Sci. 26 (2001) 341–344.
[7] A.W. Rutherford, A. Boussac, Water photolysis in biology, Science 303 (2004) 1782–1784.
[8] G.C. Dismukes, Y. Siderer, Intermediates of a polynuclear manganese center involved in photosynthetic oxidation of water, Proc. Natl. Acad. Sci. U. S. A. 78 (1981) 274–278.
[9] J. Bonvoisin, G. Blondin, J.-J. Girerd, J.-L. Zimmermann, Theoretical study of the multiline E.P.R. Signal from the S_2 state of the oxygen evolving complex of Photosystem II. Evidence for a magnetic tetramer, Biophys. J. 61 (1992) 1076–1086.
[10] J.M. Peloquin, R.D. Britt, EPR/ENDOR characterization of the physical and electronic structure of the OEC Mn cluster, Biochim. Biophys. Acta 1503 (2001) 96–111.
[11] T.G. Carrell, A.M. Tyryshkin, G.C. Dismukes, An evaluation of structural models for the photosynthetic water-oxidizing complex derived from spectroscopic and X-ray diffraction signatures, J. Biol. Inorg. Chem. 7 (2002) 2–22.
[12] K. Hasegawa, T.-A. Ono, Y. Inoue, M. Kusunoki, Spin–exchange interactions in the S_2-state manganese tetramer in photosynthetic oxygen-evolving complex deduced from g=2 multiline EPR signal, Chem. Phys. Lett. 300 (1999) 9–19.
[13] K. Hasegawa, T.-A. Ono, Y. Inoue, M. Kusunoki, How to evaluate the structure of a tetranuclear Mn cluster from magnetic and EXAFS data: case of the S_2-state Mn-cluster in Photosystem II, Bull. Chem. Soc. Jpn. 72 (1999) 1013–1023.
[14] R.D. Britt, Oxygen evolution, in: D.R. Ort, C.F. Yocum (Eds.), Oxygenic Photosynthesis: The Light Reactions, Kluwer Academic Publishers, Dordrecht, The Netherlands, 1996, pp. 137–164.
[15] R.J. Debus, The manganese and calcium ions of photosynthetic oxygen evolution, Biochim. Biophys. Acta 1102 (1992) 269–352.

[16] A.W. Rutherford, Photosystem II, the water-splitting enzyme, Trends Biochem. Sci. 14 (1989) 227–232.
[17] A.W. Rutherford, J.-L. Zimmermann, A. Boussac, Oxygen evolution, in: J. Barber (Ed.), Topics in Photosynthesis, Vol. 11: The Photosystems: Structure, Function and Molecular Biology, Elsevier Science Publishers, Amsterdam, The Netherlands, 1992, pp. 179–229.
[18] V.K. Yachandra, K. Sauer, M.P. Klein, Manganese cluster in photosynthesis: where plants oxidize water to dioxygen, Chem. Rev. 96 (1996) 2927–2950.
[19] G.W. Brudvig, EPR spectroscopy of manganese enzymes, in: A.J. Hoff (Ed.), Advanced EPR: Applications in Biology and Chemistry, Elsevier, Amsterdam, The Netherlands, 1989, pp. 839–864.
[20] G.C. Dismukes, Polynuclear manganese enzymes, in: J. Reedijk (Ed.), Bioinorganic Catalysis, Marcel Dekker, New York, 1993, pp. 317–346.
[21] A. Boussac, H. Kuhl, E. Ghibaudi, M. Rögner, A.W. Rutherford, Detection of an electron paramagnetic resonance signal in the S_0 state of the manganese complex of Photosystem II from *Synechococcus elongatus*, Biochemistry 38 (1999) 11942–11948.
[22] V.J. DeRose, V.K. Yachandra, A.E. McDermott, R.D. Britt, K. Sauer, M.P. Klein, Nitrogen ligation to manganese in the photosynthetic oxygen-evolving complex: continuous-wave and pulsed EPR studies of Photosystem II particles containing ^{14}N or ^{15}N, Biochemistry 30 (1991) 1335–1341.
[23] A.E. McDermott, V.K. Yachandra, R.D. Guiles, J.L. Cole, S.L. Deiheimer, R.D. Britt, K. Sauer, M.P. Klein, Characterization of the manganese O_2-evolving complex and the iron-quinone acceptor complex in Photosystem II from a thermophilic cyanobacterium by electron paramagnetic resonance and X-ray absorption spectroscopy, Biochemistry 27 (1988) 4021–4031.
[24] D.L. Kirilovsky, A. Boussac, F.J.E. van Mieghem, J.-M.R.C. Ducruet, P. Sétif, J. Yu, W.F.J. Vermaas, A.W. Rutherford, Oxygen-evolving Photosystem II preparation from wild type and Photosystem II mutants of *Synechocystis* sp, PCC 6803, Biochemistry 31 (1992) 2099–2107.
[25] G.H. Noren, R.J. Bœrner, B.A. Barry, EPR characterization of an oxygen-evolving Photosystem II preparation from the transformable cyanobacterium *Synechocystis* 6803, Biochemistry 30 (1991) 3943–3950.
[26] X.-S. Tang, B.A. Diner, Biochemical and spectroscopic characterization of a new oxygen-evolving Photosystem II core complex from the cyanobacterium synechocystis PCC 6803, Biochemistry 33 (1994) 4594–4603.
[27] A.W. Rutherford, M. Seibert, J.G. Metz, Characterisation of the low-fluorescent (LF1) mutant of *Scenedesmus* by EPR, Biochim. Biophys. Acta 932 (1988) 171–176.
[28] H. Schiller, S. Klingelhöfer, W. Dörner, H. Senger, H. Dau, Comparison of structure and function of the photosynthetic oxygen-evolving complex of spinach and the green alga *Scenedesmus obliquus*, in: P. Mathis (Ed.), Photosynthesis: From Light to Biosphere, Kluwer Academic Publishers, The Netherlands, 1995, pp. II463–II466.
[29] J.L. Casey, K. Sauer, EPR detection of a cryogenically photogenerated intermediate in photosynthetic oxygen evolution, Biochim. Biophys. Acta 767 (1984) 21–28.
[30] J.-L. Zimmermann, A.W. Rutherford, Electron paramagnetic resonance properties of the S_2 state of the oxygen-evolving complex of Photosystem II, Biochemistry 25 (1986) 4609–4615.
[31] J.-L. Zimmermann, A.W. Rutherford, EPR studies of the oxygen-evolving enzyme of Photosystem II, Biochim. Biophys. Acta 767 (1984) 160–167.
[32] K. Lindberg, L.-E. Andréasson, A one-site, two-state model for the binding of anions in Photosystem II, Biochemistry 35 (1996) 14259–14267.
[33] P. van Vliet, A.W. Rutherford, Properties of the chloride-depleted oxygen-evolving complex of Photosystem II studied by electron paramagnetic resonance, Biochemistry 35 (1996) 1829–1839.
[34] T.-A. Ono, H. Nakayama, H. Gleiter, Y. Inoue, A. Kawamori, Modification of the properties of the S_2 state in photosynthetic oxygen-evolving center by replacement of chloride with other anions, Arch. Biochem. Biophys. 256 (1987) 618–624.
[35] P. van Vliet, Landbouwuniversiteit Wageningen, 1996.
[36] W.F. Beck, J.C. de Paula, G.W. Brudvig, Ammonia binds to the manganese site of the O_2-evolving complex of Photosystem II in the S_2 state, J. Am. Chem. Soc. 108 (1986) 4018–4022.
[37] A. Boussac, A.W. Rutherford, Nature of the inhibition of the oxygen-evolving enzyme of Photosystem II induced by NaCl washing and reversed by the addition of Ca^{2+} or Sr^{2+}, Biochemistry 27 (1988) 3476–3483.
[38] A. Boussac, J.-J. Girerd, A.W. Rutherford, Conversion of the spin state of the manganese complex in Photosystem II induced by near-infrared light, Biochemistry 35 (1996) 6984–6989.
[39] A. Boussac, H. Kuhl, S. Un, M. Rögner, A.W. Rutherford, Effect of near-infrared light on the S_2-state of the manganese complex of Photosystem II from *Synechococcus elongatus*, Biochemistry 37 (1998) 8995–9000.
[40] A. Boussac, S. Un, O. Horner, A.W. Rutherford, High-spin states ($S \geq 5/2$) of the Photosystem II manganese complex, Biochemistry 37 (1998) 4001–4007.
[41] O. Horner, E. Rivière, G. Blondin, S. Un, A.W. Rutherford, J.-J. Girerd, A. Boussac, SQUID magnetization study of the infrared-induced spin transition in the S_2 state of Photosystem II: spin value associated with the g=4.1 EPR signal, J. Am. Chem. Soc. 120 (1998) 7924–7928.
[42] A. Boussac, Inhomogeneity of the EPR multiline signal from the S_2-state of the Photosystem II oxygen-evolving enzyme, J. Biol. Inorg. Chem. 2 (1997) 580–585.
[43] D.A. Force, D.W. Randall, G.A. Lorigan, K.L. Clemens, R.D. Britt, ESEEM studies of alcohol binding to the manganese cluster of the oxygen evolving complex of Photosystem II, J. Am. Chem. Soc. 120 (1998) 13321–13333.
[44] K. Hasegawa, M. Kusunoki, Y. Inoue, T.-A. Ono, Simulation of S_2-state multiline EPR signal in oriented Photosystem II membranes: structural implications for the manganese cluster in an oxygen-evolving complex, Biochemistry 37 (1998) 9457–9465.
[45] M. Zheng, G.C. Dismukes, Orbital configuration of the valence electrons, ligand field symmetry, and manganese oxidation states of the photosynthetic water oxidizing complex: analysis of the S_2 state multiline EPR signals, Inorg. Chem. 35 (1996) 3307–3319.
[46] J.M. Peloquin, K.A. Campbell, D.W. Randall, M.A. Evanchik, V.L. Pecoraro, W.H. Armstrong, R.D. Britt, ^{55}Mn ENDOR of the S_2-state multiline EPR signal of Photosystem II: implications on the structure of the tetranuclear Mn cluster, J. Am. Chem. Soc. 122 (2000) 10926–10942.
[47] K.V. Lakshmi, S.S. Eaton, G.R. Eaton, H.A. Frank, G.W. Brudvig, Analysis of dipolar and exchange interactions between manganese and tyrosine Z in the $S_2Y_Z^{\bullet}$ state of acetate-inhibited Photosystem II via EPR spectral simulations at X- and Q-bands, J. Phys. Chem., B 102 (1998) 8327–8335.
[48] A. Boussac, A.W. Rutherford, S. Styring, Interaction of ammonia with the water splitting enzyme of Photosystem II, Biochemistry 29 (1990) 24–32.
[49] G. Blondin, R. Davydov, C. Philouze, M.-F. Charlot, S. Styring, B. Akermark, J.-J. Girerd, A. Boussac, EPR study of the S=1/2 ground state of a radiolysis-generated $Mn(III)M(IV)_3$ form of $[Mn^{III}{}_{V}{}_{4}O_6(bpy)_6]^{4+}$. Comparison with the photosynthetic oxygen evolving complex, J. Chem. Soc., Dalton Trans. (1997) 4069–4074.
[50] A. Bencini, D. Gatteschi, EPR of Exchange Coupled Systems, Springer-Verlach, Berlin, 1990.
[51] K.A. Åhrling, R.J. Pace, Simulation of the S_2 state multiline electron paramagnetic resonance signal of Photosystem II: a multifrequency approach, Biophys. J. 68 (1995) 2081–2090.
[52] A.W. Rutherford, A. Boussac, J.-L. Zimmermann, EPR studies of the oxygen evolving enzyme, New J. Chem. 15 (1991) 491–500.

[53] R.D. Britt, G.A. Lorigan, K. Sauer, M.P. Klein, J.-L. Zimmermann, The g=2 multiline EPR signal of the S_2 state of the photosynthetic oxygen-evolving complex originates from a ground spin state, Biochim. Biophys. Acta 1140 (1992) 95–101.
[54] M. Weissbluth, Atoms and Molecules, student edition, Academic Press, Inc., San Diego, California 92101, 1978.
[55] R.P. Scaringe, D.J. Hodgson, W.E. Hatfield, The coupled representation matrix of the pair Hamiltonian, Mol. Phys. 35 (1978) 701–713.
[56] M. Zheng, S.V. Khangulov, G.C. Dismukes, V.V. Barynin, Electronic structure of dimanganese(II,III) and dimanganese(III,IV) complexes and dimanganese catalase enzyme: a general EPR spectral simulation approach, Inorg. Chem. 33 (1994) 382–387.
[57] K.-O. Schäfer, R. Bittl, W. Zweygart, F. Lendzian, G. Haselhorst, T. Weyhermüller, K. Wieghardt, W. Lubitz, Electronic structure of antiferromagnetically coupled dinuclear manganese ($Mn^{III}Mn^{IV}$) complexes studies by magnetic resonance techniques, J. Am. Chem. Soc. 120 (1998) 13104–13120.
[58] W.B. Euler, Exact results for EPR g and A Tensors in the S_1=1, 3/2, 2, 5/2 and S_2=1/2 spin-coupled systems. The effect when S is not a good quantum number, Inorg. Chem. 25 (1986) 1871–1875.
[59] J.T. Sage, Y.-M. Xia, P.G. Debrunner, D.T. Keough, J. de Jersey, B. Zerner, Mössbauer analysis of the binuclear iron site in purple acid phosphatase from pig allantoic fluid, J. Am. Chem. Soc. 111 (1989) 7239–7247.
[60] M. Kusunoki, A new paramagnetic hyperfine structure effect in manganese tetramers. The origin of "multiline" EPR signals from an S_2 state of a photosynthetic water-splitting enzyme, Chem. Phys. Lett. 197 (1992) 108–116.
[61] M.I. Belinskii, Heisenberg model of tetrameric manganese cluster of S_2 center of Photosystem II, Chem. Phys. 179 (1994) 1–22.
[62] A. Haddy, G.S. Waldo, R.H. Sands, J.E. Penner-Hahn, Simulation of multifrequency EPR Spectra from Mn(III)/Mn(IV) catalase of *Lactobacillus plantarum* using a new approach based on perturbation theory, Inorg. Chem. 33 (1994) 2677–2682.
[63] K.-O. Schäfer, R. Bittl, F. Lendzian, V.V. Barynin, T. Weyhermüller, K. Wieghardt, W. Lubitz, Multifrequency EPR investigation of dimanganese catalase and related Mn(III)Mn(IV) complexes, J. Phys. Chem., B 107 (2003) 1242–1250.
[64] J.M. Peloquin, K.A. Campbell, R.D. Britt, ^{55}Mn pulsed ENDOR demonstrates that the Photosystem II "Split" EPR signal arises from a magnetically-coupled mangano–tyrosyl complex, J. Am. Chem. Soc. 120 (1998) 6840–6841.
[65] V.K. Yachandra, Structure of the manganese complex in Photosystem II: insights from X-ray spectroscopy, Philos. Trans. R. Soc. Lond., B 357 (2002) 1347–1358.
[66] U. Bergmann, M.M. Grush, C.R. Horne, P. DeMarois, J.E. Penner-Hahn, C.F. Yocum, D.W. Wright, C.E. Dubé, W.H. Armstrong, G. Christou, H.J. Eppley, S.P. Cramer, Characterization of the Mn oxidation states in Photosystem II by Kβ X-ray fluorescence spectroscopy, J. Phys. Chem., B 102 (1998) 8350–8352.
[67] G. Schansker, C. Goussias, V. Petrouleas, A.W. Rutherford, Reduction of the Mn cluster of the water-oxidizing enzyme by nitric oxide: formation of an S_{-2} state, Biochemistry 41 (2002) 3057–3064.
[68] J. Messinger, G. Seaton, T. Wydrzynski, U. Wacker, G. Renger, S_{-3} state of the water oxidase in Photosystem II, Biochemistry 36 (1997) 6862–6873.
[69] C. Hureau, PhD thesis in Chemistry, Paris XI, Orsay, France, 2003.
[70] O. Horner, M.-F. Charlot, A. Boussac, E. Anxolabéhère-Mallart, L. Tchertanov, J. Guilhem, J.-J. Girerd, Synthesis, structure, electronic, redox, and magnetic properties of a new mixed valent Mn-Oxo cluster: $[Mn_2^{III,IV}O_2(N,N\text{-bispicen})_2]^{3+}$ (*N,N*-bispicen=*N,N*-bis(2-pyridylmethyl)-1,2-diaminoethane, Eur. J. Inorg. Chem. (1998) 721–727.
[71] O. Horner, E. Anxolabéhère-Mallart, M.-F. Charlot, L. Tchertanov, J. Guilhem, T.A. Mattioli, A. Boussac, J.-J. Girerd, A new manganese dinuclear complex with phenolate ligands and a single unsupported oxo bridge. Storage of two positive charges within less than 500 mV. Relevance to photosynthesis, Inorg. Chem. 38 (1999) 1222–1232.
[72] C. Hureau, L. Sabater, E. Anxolabéhère-Mallart, M. Nierlich, M.-F. Charlot, F. Gonnet, E. Rivière, G. Blondin, Synthesis, structure and characterisation of a new phenolato-bridged manganese complex $[(mL)_2Mn_2]^{2+}$. Chemical and electrochemical access to a new Mono-mu-Oxo dimanganese core unit, Chem. Eur. J. (2003) 1998–2010.
[73] P.L.W. Tregenna-Piggott, H. Weihe, A.-L. Barra, High-field, multi-frequency EPR study of the $[Mn(OH_2)_6]^{3+}$ cation: influence of π-bonding on the ground state zero-field-splitting parameters, Inorg. Chem. 42 (2003) 8504–8508.
[74] H.J. Gerritsen, E.S. Sabisky, Paramagnetic resonance of trivalent manganese in rutile (TiO_2), Phys. Rev. 132 (1963) 1507–1512.
[75] A.-L. Barra, D. Gatteschi, R. Sessoli, G.L. Abbati, A. Cornia, A.C. Fabretti, M.G. Uytterhoeven, Electronic structure of Manganese(III) compounds from high-frequency EPR spectra, Angew. Chem., Int. Ed. Engl. 36 (1997) 2329–2331.
[76] K.A. Campbell, E. Yikilmaz, C.V. Grant, W. Gregor, A.-F. Miller, R.D. Britt, Parallel polarization EPR characterization of the Mn(III) center of oxidized manganese superoxide dismutase, J. Am. Chem. Soc. 121 (1999) 4714–4715.
[77] K.A. Campbell, D.A. Force, P.J. Nixon, F. Dole, B.A. Diner, R.D. Britt, Dual-mode EPR detects the initial intermediate in photo-assembly of the Photosystem II Mn cluster: the influence of amino acid residue 170 of the D1 polypeptide on Mn coordination, J. Am. Chem. Soc. 122 (2000) 3754–3761.
[78] J. Limburg, J.S. Vrettos, R.H. Crabtree, G.W. Brudvig, J.C. de Paula, A. Hassan, A.-L. Barra, C. Duboc-Toia, M.-N. Collomb, High-frequency EPR study of a new mononuclear manganese(III) complex: $[(terpy)Mn(N_3)_3]$ (terpy=2,2′:6′,2″-terpyridine), Inorg. Chem. 40 (2001) 1698–1703.
[79] K.A. Campbell, M.R. Lashley, J.K. Wyatt, M.H. Nantz, R.D. Britt, Dual-mode EPR study of Mn(III) salen and the Mn(III) salen-catalyzed epoxidation of *cis*-β-methylstyrene, J. Am. Chem. Soc. 123 (2001) 5710–5719.
[80] J. Krzystek, J. Telser, B.M. Hoffman, L.-C. Brunel, S. Licoccia, High-frequency and field EPR investigation of (8,12-diethyl-2,3,7,13,17,18-hexamethylcorrolato)manganese(III), J. Am. Chem. Soc. 123 (2001) 7890–7897.
[81] J. Krzystek, J. Telser, L.A. Pardi, D.P. Goldberg, B.M. Hoffman, L.-C. Brunel, High-frequency and -field electron paramagnetic resonance of high-spin manganese(III) in porphyrinic complexes, Inorg. Chem. 38 (1999) 6121–6129.
[82] C. Mantel, A.K. Hassan, J. Pécaut, A. Deronzier, M.-N. Collomb, C. Duboc-Toia, A high-frequency and high-field EPR study of new azide and fluoride mononuclear Mn(III) complexes, J. Am. Chem. Soc. 125 (2003) 12337–12344.